Naphthalimide-Annulated [*n*]Helicenes: Red Circularly Polarized Light Emitters

Xiaoqi Tian,[a] Kazutaka Shoyama,[a] Bernhard Mahlmeister,[b] Felix Brust[b], Matthias Stolte[a,b], Frank Würthner[a, b, *]

[a]Institut für Organische Chemie, Universität Würzburg, Am Hubland, 97074 Würzburg, Germany; [b]Center for Nanosystems Chemistry (CNC), Universität Würzburg, Theodor-Boveri-Weg, 97074 Würzburg, Germany.

Keywords: Helicene, naphthalimide, fluorescence, circularly polarized luminescence brightness.

ABSTRACT: Two [*n*]heliceno-bis(naphthalimides) **1** and **2** (*n* = 5 and 6, respectively) where two electron-accepting naphthalimide moieties are attached at both ends of helicene core were synthesized by effective two-step strategy and their enantiomers could be resolved by chiral stationary phase HPLC. The single-crystal X-ray diffraction analysis of enantiopure fractions of **1** and **2** confirmed their helical structure, and together with experimental and calculated circular dichroism (CD) spectra the absolute configuration was unambiguously assigned. Both **1** and **2** exhibit high molar extinction coefficients for the S_0–S_1 transition and high fluorescence quantum yields (73% for **1** and 69% for **2**), both being outstanding for helicene derivatives. The red circularly polarized luminescence (CPL) emission up to 615 nm for **2** with CPL brightness (B_{CPL}) up to 66.5 M^{-1} cm^{-1} demonstrates its potential for applications in chiral optoelectronics. TD-DFT calculations unambiguously showed that the large transition magnetic dipole moment $|m|$ of **2** is responsible for its high absorbance dissymmetry (g_{abs}) and luminescence dissymmetry (g_{lum}) factor

INTRODUCTION

Helicenes are *ortho*-fused helically chiral polycyclic aromatic hydrocarbons.[1-4] This distinct class of compounds show excellent chiroptical properties because of their inherent helical chirality, which endows them the potential for applications in asymmetric catalysis,[5] organic electronics,[6-8] and molecular machines.[9-10] Their thermal and chemical stability make themselves suitable chiral light-emitting materials,[11-12] for which both emission quantum yield (Φ_{PL}) and luminescence dissymmetry factor (g_{lum}) should be maximized. These factors together with extinction coefficient (ϵ_{max}) define one of the most important properties of chiral functional materials, CPL brightness (B_{CPL}), which is defined as $B_{CPL} = \epsilon_{max} \times \Phi_{PL} \times |g_{lum}|/2$.[13] Helicene-based materials have high absorption coefficients and sufficiently high dissymmetry factors originating from their effective π-conjugation and intrinsically chiral nature. However, low fluorescence quantum yield caused by fast intersystem crossing from the singlet excited to the triplet state is a major obstacle for the application of helicenes as light emitting materials (the fluorescence quantum yields of pristine [5]helicene and [6]helicene are only 4%).[14-16] This problem is even more severe at longer emission wavelengths, i.e. > 600 nm, since the fluorescence quantum yield decreases due to faster vibrational relaxation.[17] In general, two main strategies have been used to improve the fluorescence quantum yields. The first one is the introduction of appropriate substituents or heteroatom-doping (e.g. **H1**, Figure 1,).[18-22] Adding electron-donating or withdrawing groups or replacing carbon by heteroatoms at appropriate positions changes the energy levels of frontier molecular orbitals which eventually alters the optical properties. The other strategy is a lateral π-extension of the helicene-backbone.[23-32] Along this strategy the groups of Nuckolls and Wang have made use of the favourable optical and redox properties of perylene bisimide (PBI) emitters and reported in recent years helicene–PBI hybrid molecules with high fluorescence quantum yields and optimal dissymmetry factors (Figure 1, **H2**, **H3**).[33-39] However, those helicene–PBI hybrids possess low absorption coefficients originating from localized HOMO and LUMO orbitals with small overlap that afford only modest CPL brightness. Therefore, the design of π-extended helicenes with high CPL brightness in red-light region, whose high g_{abs} and g_{lum} are originating from helicene, and high fluorescence quantum yield and molar extinction coefficient for the S_0–S_1 transition originating from perylene dyes remains an elusive goal.

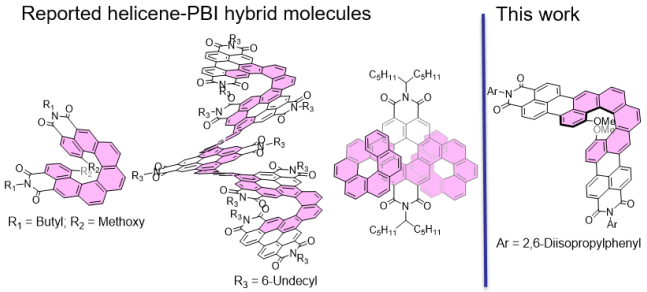

	H1	H2	H3	2
g_{lum}	-[a]	-[a]	2 × 10^{-3}	2.3 × 10^{-3}
Φ_{PL}	12%	68%	33%	69%
ϵ_{max}	7000	60000	26300	84300
B_{CPL}	-[a]	-[a]	8.7	66.5

Figure 1. Helicene-based emitters and their g_{lum}, fluorescence quantum yield, absorption coefficient for the S_0–S_1 transition (M^{-1} cm^{-1}), and CPL brightness (M^{-1} cm^{-1}). Helicene moieties in each structure are highlighted in color. [a] not reported.

In this work, we present a new strategy of two-fold palladium-catalyzed [3 + 3] naphthalimide-annulation of [*n*]helicenes (*n* = 5 and 6).[40-41] The obtained perylene imide (PMI)-helicene-PMI molecules possess delocalized HOMO−1, HOMO, LUMO and LUMO+1 as confirmed by time-dependent density functional theory (TD-DFT) calculations, thereby exhibiting strongly allowed S_0–S_1 absorption and red emission. Furthermore, CD and CPL measurements revealed their high dissymmetry factors, which originate from the helicene backbone. Such highly emissive helicene molecules are promising for applications as self-assembled emitter materials, in bio-imaging or as chiral photodetectors.[42-43]

SCHEME 1. Synthesis of naphthalimide-annulated [*n*]helicenes 1 and 2[a]

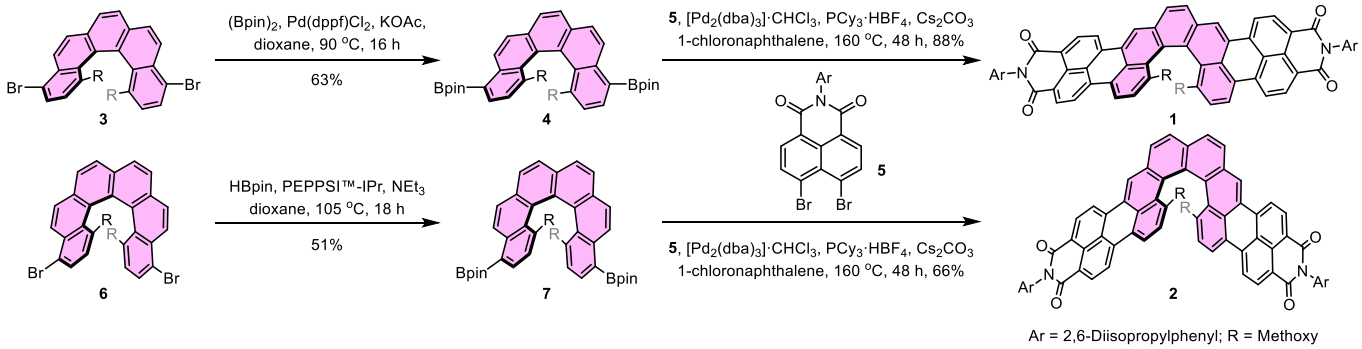

[a]dppf: 1,1'-bis(diphenylphosphino)ferrocene, dba: dibenzylideneacetone, pin: pinacolato, Cy: cyclohexyl, PEPPSI™-IPr: (3-chlorpyridyl)-(1,3-diisopropylimidazol-2-ylidene)-palladium(II)-dichloride

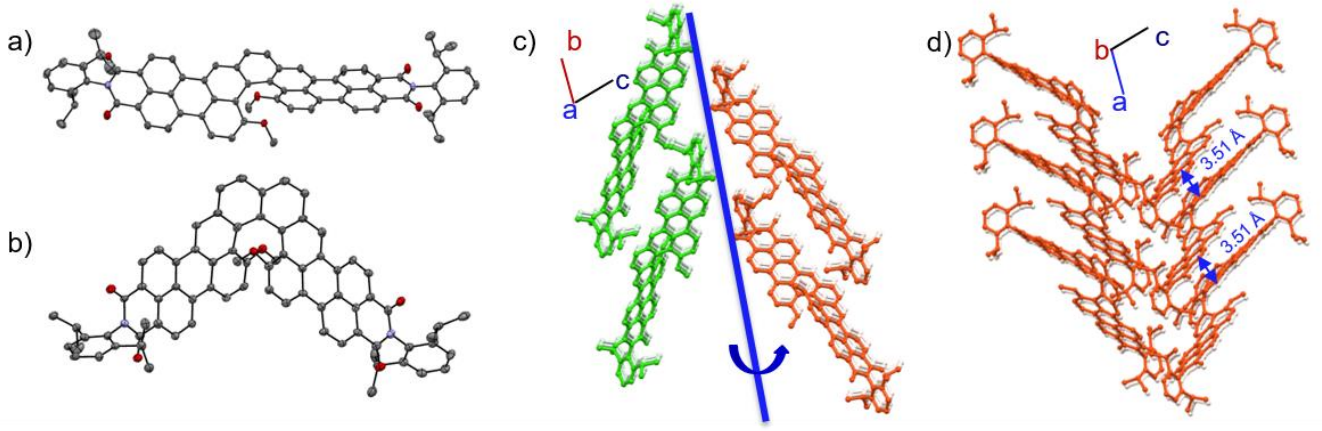

Figure 2. a, b) Molecular structures of *M*-**1** and *M*-**2** determined by X-ray diffraction analysis of second HPLC fractions of **1** and **2**. ORTEP drawings are shown with 50% probability for *M*-**1** and 15% probability for *M*-**2**. c, d) Packing arrangements of *M*-**1** (the two-fold screw axis showed in blue) and *M*-**2**. Solvent molecules and hydrogen atoms are omitted for clarity.

RESULTS AND DISCUSSION

Synthesis

The syntheses of **1** and **2** were achieved by a two-step strategy from literature-known compounds 7,14-dibromo-10,11-dimethoxy[5]helicene **3**[44] or 9,16-dibromo-12,13-dimethoxy[6]helicene **6**[45-47], respectively (Scheme 1). The key reaction of this strategy is a palladium-catalyzed [3 + 3] annulation.[40-41] The synthesis of compound **1** started from Miyaura borylation of **3** using $Pd(dppf)Cl_2$ as the catalyst, bis(pinacolato)diboron as the borylation reagent and KOAc as the base, which afforded 10,11-dimethoxy[5]helicene-7,14-diboronic ester **4** in a good yield of 63%. In the final key step, a twofold palladium-catalyzed [3 + 3] annulation reaction between **4** and dibromonaphthalene dicarboximide **5** using $[Pd_2(dba)_3]\cdot CHCl_3$ as the catalyst, $PCy_3\cdot HBF_4$ as the ligand, and Cs_2CO_3 as the base in 1-chloronaphthalene afforded naphthalimide-annulated [5]helicene **1** in an excellent yield of 88% as a purple solid. For the synthesis of [6]helicene derivative **2**, the equivalent Miyaura borylation reaction for **6** afforded the desired product **7** only in 17% isolated yield. After extensive optimization of the reaction conditions we found that boronic ester **7** could be isolated in 51% yield using PEPPSI™-IPr[48] as the catalyst, HBpin as the borylation reagent, and a mixture of NEt_3 and dioxane as the solvent.[49] In the final step, the twofold palladium-catalyzed [3 + 3] annulation reaction was applied again to afford [6]helicene derivative **2** in 66% yield. Both compounds **1** and **2** showed high stability under ambient light in air at room temperature as well as good solubility in various solvents such as chloroform and THF. The structures of those two compounds were unambiguously characterized using NMR, high-resolution mass spectra, and single-crystal X-ray diffraction analysis. Enantiopure fractions of **1** and **2** could be obtained by recycling semi-preparative HPLC (details in SI). The absolute configurations of the isolated isomers were assigned using CD spectroscopy and TD-DFT calculations (for both **1** and **2** the first fractions obtained after chiral stationary

phase HPLC separation were assigned as *P*). For **1**, absolution configuration could also be substantiated by X-ray crystallographic analysis.

Structural Properties

To confirm the helical structure of newly synthesized imide derivatives, single crystals for X-ray crystallographic analysis were grown by slow evaporation of hexane into a dichloroethane solution of first and second HPLC fractions of **1** and **2**. As shown in Figure 2a, the absolute configuration of the second HPLC fraction of **1** was unambiguously assigned as *M*, which was further proved by comparison of the experimental with the calculated CD spectra (*vide infra*). [5]Helicene derivative *M*-**1** crystallizes in the non-centrosymmetric monoclinic space group $P2_1$, with a torsional angle of 23.6° in the inner helix (Figure 2a), which is slightly smaller than that of 7,14-dibromo-10,11-dimethoxy[5]helicene **3** (25.5°).[44] In contrast to the dimeric packing found in the crystal structure of racemic *rac*-**1** (Figure S17a and S17b), crystals grown from enantiopure fractions of **1** indicated that they crystallize in zig-zag arrangement along the *c*-axis with a slipped-stack arrangement along the *a*-axis but without any π–π interactions (Figure 2c). [6]helicene derivative *M*-**2** crystallizes in the non-centrosymmetric triclinic space group *P*1 with two crystallographic isomers facing toward two different directions in each unit cell. The torsion angle in the inner helix of *M*-**2** was determined as 25.0° (Figure 2b), which is slightly larger than that of *M*-**1**. Unlike the packing structure of *rac*-**2**, where the (*P*)- and (*M*)-enantiomers form a dimer through π–π interactions with an average π–π distances of approximately 3.54 Å (Figure S17c and S17d), crystals grown from enantiopure fraction of *M*-**2** (absolute configuration determined by CD, *vide infra*) crystallize in slipped-stack arrangement along the *a*-axis with a close π–π distance of 3.51 Å (Figure 2d). The chiral crystal structure and the different crystallographic symmetry for these two similar molecules ($P2_1$ for **1**, *P*1 for **2**) might be of interest for nonlinear optical technologies.[50]

Electrochemical Properties

Both **1** and **2** were electrochemically characterized by cyclic voltammetry (CV) and square-wave voltammetry (SWV) in dichloromethane using Bu_4NPF_6 as supporting electrolyte (Figure 3). Traces of CV and SWV revealed that **1** showed two well-defined reversible one-electron oxidation processes with half-wave potentials of E_{ox1} = 0.60 V and E_{ox2} = 0.92 V. For reduction, a reversible two-electron (about twice the height of the one-electron waves) and a subsequent one-electron process with half-wave potentials of $E_{red1/2}$ = –1.38 V and E_{red3} = –2.12 V were observed within the scanning range. Similarly, [6]helicene derivative **2** shows two reversible oxidative processes with E_{ox1} = 0.67 V and E_{ox2} = 0.85 V. For reduction, three one-electron reduction processes with half-wave potentials of E_{red1} = –1.47 V, E_{red2} = –1.56 V, and E_{red3} = –2.00 V were observed. Interestingly, the potential difference between the two reduction peaks (ΔE_{red}) of **1** is ~0 V while the ΔE_{red} of **2** is 0.09 V. This is in stark contrast to rylene bisimides where ΔE_{red} decreases with an increase of π-conjugation.[51] Through-bond conjugation plays the major role for rylene bisimides whilst intramolecular through-space interaction becomes the key factor in our system due to the close distance of the two charged PMI moieties. The trend observed in our system is also different from that observed for previously reported [*n*]helicene bisimides, i.e. **H1** for *n* = 7, where [5]/[6]helicene bisimide derivatives still followed the trend of rylene bisimides and the effect of intramolecular through-space interaction appeared only for the [7]helicene bisimide derivative.[22] Accordingly, the electrochemical energy gaps were thus calculated to be 1.98 and 2.14 eV for **1** and **2**, respectively.

Absorption and Fluorescence Properties

To elucidate the optical properties of **1** and **2**, their UV/vis absorption and emission spectra were recorded in chloroform at room temperature (Figure 4 and Table 1). Both compounds exhibit strong well-structured peaks for the longest-wavelength absorption in the 550–670 nm region and weak rather unresolved peaks in the 300–450 nm region, which are the characteristics of perylene and helicene subunits,

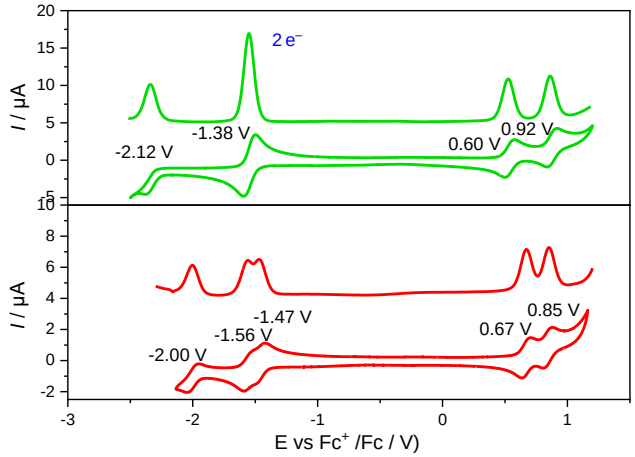

Figure 3. CV and SWV plots of **1** (green) and **2** (red) vs Fc/Fc^+ redox couple in dichloromethane with a supporting electrolyte, $[Bu_4N][PF_6]$ (0.1 M), at a scan rate of 100 mV/s.

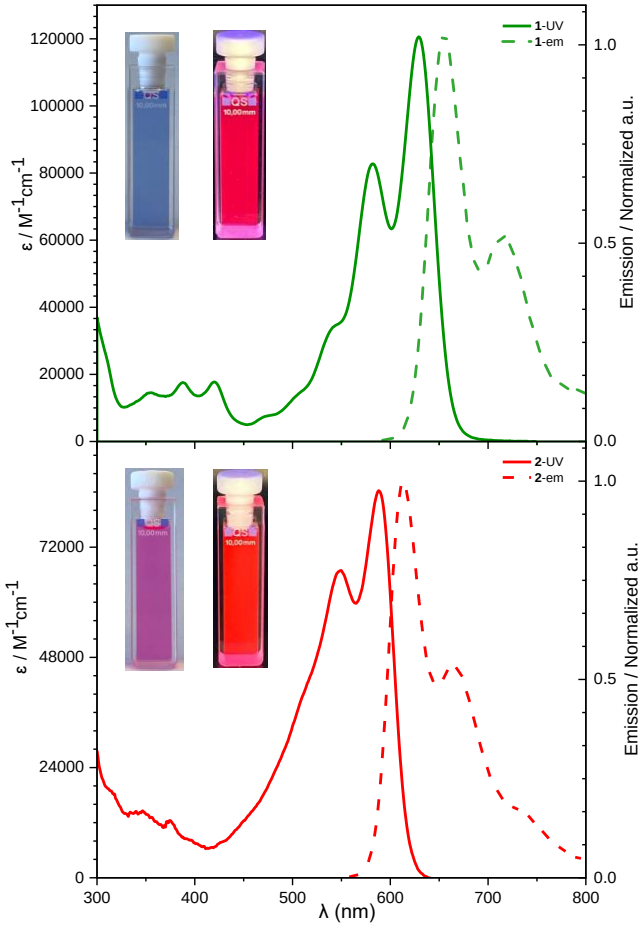

Figure 4. UV−vis absorption and normalized fluorescence spectra of **1** (green) and **2** (red) in chloroform solution ($c \sim 4 \times 10^{-6}$ M for

UV–vis, OD ~ 0.05 for fluorescence) at 293 K. Fluorescence data [λ_{ex}(**1**) = 581 nm, λ_{ex}(**2**) = 548 nm]. Insets: Photographs of chloroform solutions under ambient light (left) and under UV light (right).

Table 1. Summary of Optical Properties of **1** and **2**

	λ_{abs} [nm][a]	λ_{em} [nm][b]	ϵ_{max} [M^{-1} cm^{-1}]	Φ_{PL} (%)[c]	t [ns]	E_g^{opt} [eV][d]	E_g^{ec} [eV][e]
1	629	655	120600	73	2.64	1.86	1.98
2	588	613	84300	69	3.40	2.02	2.14

[a]Measured in chloroform (4×10^{-6} M). [b]Measured in chloroform (OD ~ 0.05) [c]Determined as average value of four different excitation wavelengths relative using *N*,*N*'-bis(2,6-diisopropyl-phenyl)-1,6,7,12-tetraphenoxy-perylene-3,4:9,10-bis(dicarboximide) (Φ_{PL} = 0.96 in chloroform) as standards under highly diluted conditions (OD ≤ 0.05) and magic angle conditions (54.7°). [d]Calculated by the onset of absorption in a chloroform solution according to E_g^{opt} (eV) = (1240/λ_{onset}). [e]Calculated using the equations $E_g^{ec} = E_{LUMO} - E_{HOMO}$, $E_{LUMO} = -[E(M/M^-) + 5.15]$ and $E_{HOMO} = -[E(M/M^+) + 5.15]$, assuming that the energy level of Fc^+/Fc with respect to the vacuum level is −5.15 eV.

respectively. In addition, the absorption coefficients in the long-wavelength region (550−670 nm) are comparable or even higher than those of PBI with values in the range of 84300−120600 M^{-1} cm^{-1}. However, the absorption intensity associated with the helicene subunits diminishes. This is in stark contrast to the previously reported helicene−PBI hybrid molecules, whose maximum absorption peaks originated from the helicene subunits.[33-39] This difference could be explained by TD-DFT calculations, which showed that the lowest energy absorption bands of **1** and **2** are accordingly mainly attributed to the HOMO → LUMO and HOMO−1 → LUMO+1 transitions with very high oscillator strengths (*f*) of 2.05 and 1.54, respectively (Figure 5). All those four orbitals are delocalized over the entire molecule, resulting in a single-chromophore system. On the other hand, the lowest energy absorption bands of previously reported helicene−PBI hybrid molecules[33-39] were mainly attributed to the partially allowed HOMO → LUMO transition, where the two orbitals mainly localized in the helicene and PBI units, respectively.

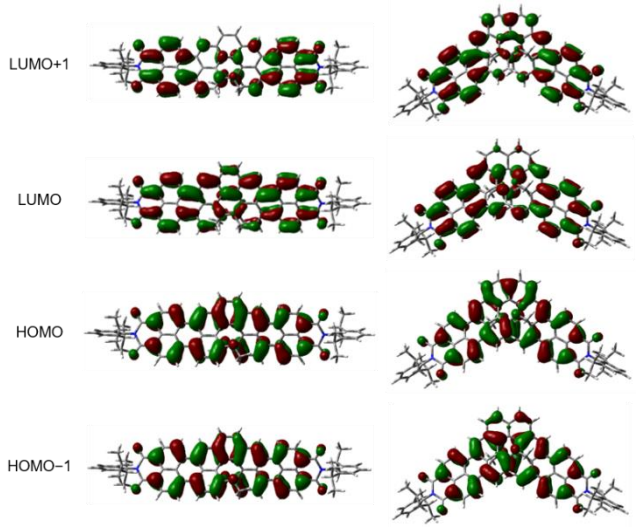

Figure 5. Selected molecular orbitals of model **1** and **2** calculated by TD-DFT at the ωB97XD/def2-svp level of theory for *P*-enantiomers.

[5]Helicene derivative **1** showed a well-resolved S_0−S_1 transition at λ_{abs} = 629 nm (ϵ_{max} = 120600 M^{-1} cm^{-1}) with a shoulder located at 582 nm and a mirror-image fluorescence with a λ_{em} of 655 nm, corresponding to a Stokes shift of 630 cm^{-1}. The fluorescence quantum yield is 73% measured via relative method, with a lifetime of 2.64 ns. [6]Helicene derivative **2** exhibits a similar band shape as **1**, however, with a hypsochromic shift with respect to **1**. The absorption maximum of **2** was at 588 nm (ϵ_{max} = 84300 M^{-1} cm^{-1}) with a shoulder at 549 nm and its emission peak (λ_{em}) centered at 613 nm, corresponding to a Stokes shift of 690 cm^{-1}. The fluorescence quantum yield and lifetime of **2** are 69% and 3.40 ns, respectively. Thanks to the high fluorescence quantum yield of the [6]helicene derivative **2**, along with the narrow-band emission in the NIR region, we employ it as a singlet emitting material in vacuum-processed organic light emitting devices (OLEDs). Red-emissive OLED devices with an EQE of up to 1.7% at a luminance of 100 cd m^{-2} and appreciably low turn-on voltages (V_{TO}) at about 4.5 V could be achieved (details in SI). As estimated from the onsets of the lowest-energy absorption band of their UV/vis absorption spectra, the optical energy gaps of **1** and **2** were calculated to be 1.86 and 2.02 eV, respectively. These values are in good accordance with their electrochemical energy gaps, which further substantiates the high degree of delocalization of frontier molecular orbitals.

Chiroptical Properties

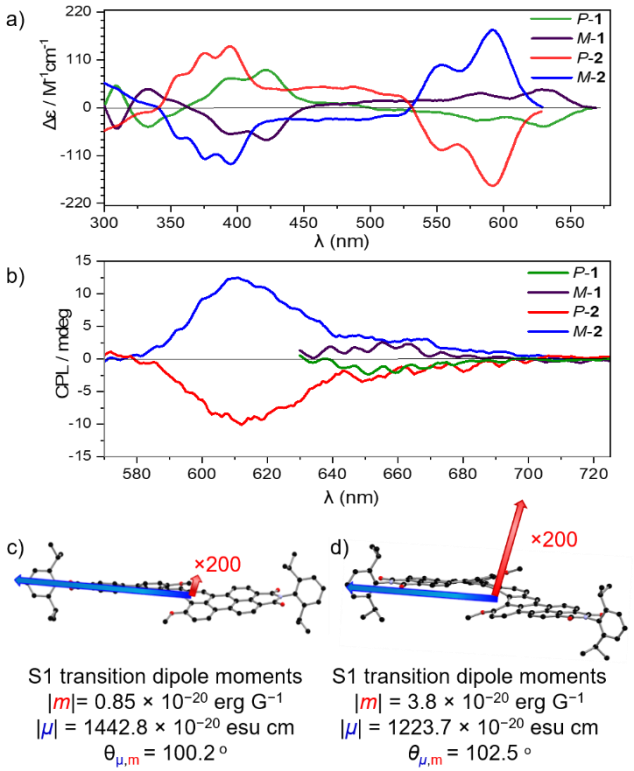

Figure 6. CD (a) and CPL (b) spectra of **1** and **2** in chloroform (*c* ~ 1×10^{-6} M) (spectra were smoothed, original spectra shown in Figure S7 and S8). S_1 transition dipole moments of *P*-**1** (c) and *P*-**2** (d), for the dipole moments, the TMDM vector is shown in red, and the TEDM vector is shown in blue.

The CD spectra of the enantiomers *P*/*M*-**1** and *P*/*M*-**2** were measured in chloroform. As shown in Figure 6a,

enantiomerically pure **1** and **2** exhibit Cotton effects in the range 300−650 nm with perfect mirror-image CD spectra (Figure 6a). The maximal $\Delta\varepsilon$ values are 86 M^{-1} cm^{-1} at 421 nm and 45 M^{-1} cm^{-1} at 630 nm for **1**, and 143 M^{-1} cm^{-1} at 396 nm and 181 M^{-1} cm^{-1} at 592 nm for **2**. In addition, the absorption dissymmetry factor g_{abs} ($g_{abs} = \Delta\epsilon/\epsilon$)) of **1** is 6.8×10^{-3} at 438 nm and 4.5×10^{-4} at 630 nm, while the g_{abs} of **2** reach to 3.2×10^{-2} at 393 nm and 2.1×10^{-3} at 594 nm. The dramatically higher value of g_{abs} for **2** was also observed in our simulated CD spectra (Figure S9 and S10). The relatively small g_{abs} in the longer wavelength region are attributed to the high extinction coefficient ϵ.

Table 2. Summary of Chiroptical Properties of the *P*-**1** and *P*-**2**

	CD[a]		S_0−S_1 transition[b]				CPL[a]	S_1−S_0 transition[b]			
	λ [nm]	$\lvert g_{abs}\rvert$	$\lvert\mu\rvert$[c]	$\lvert m\rvert$[d]	θ [deg]	$\lvert g_{abs}\rvert^{cal}$	$\lvert g_{lum}\rvert$	$\lvert\mu\rvert$[c]	$\lvert m\rvert$[d]	θ [deg]	$\lvert g_{lum}\rvert^{cal}$
1	630	4.5×10^{-4}	1443	0.85	100.2	4.2×10^{-4}	5.0×10^{-4}	1535	1.00	99.6	4.3×10^{-4}
2	594	2.1×10^{-3}	1224	3.80	102.5	2.7×10^{-3}	2.3×10^{-3}	1129	3.06	99.4	1.8×10^{-3}

[a]Measured in chloroform solutions ($c \sim 1 \times 10^{-6}$ M). [b]Calculated by TD-DFT at the ωB97XD/def2-svp level of theory for *P*-enantiomers. [c]$|\mu|$ [10^{-20} esu cm]. [d]$|m|$ [10^{-20} erg G^{-1}].

According to the theory, the dissymmetry factor for CD (g_{abs}) is described as: $g_{abs} = 4 \times |\mu| \times |m| \times \cos\theta/(|\mu|^2 + |m|^2)$,[52-53] where μ and m are the transition electric dipole moments (TEDM) and transition magnetic dipole moments (TMDM) vectors, and θ is the angle between the μ and m. The TEDM of organic molecules tends to be several hundred times larger than the TMDM, therefore, the equation can be simplified as: $g_{abs} = 4 \times \cos\theta \times |m|/|\mu|$. From the simplified equation, it is clear that the key for obtaining higher g_{abs} values are the large ratio of $|m|/|\mu|$ and a large $|\cos\theta|$. The μ and m as well as the angle (θ) between μ and m of *P*-**1** and *P*-**2** for their S_0−S_1 transitions were determined by TD-DFT calculations (Table 2). The $\cos\theta$ and $|\mu|$ of *P*-**1** and *P*-**2** are almost the same while $|m|$ of *P*-**2** is about 4.5 times higher compared to that of *P*-**1**, i. e. $|m| = 0.85 \times 10^{-20}$ erg G^{-1} for *P*-**1** and $|m| = 3.80 \times 10^{-20}$ erg G^{-1} for *P*-**2**. This difference is consistent with the trend observed experimentally, which unambiguously shows that the large magnetic transition dipole moment of *P*-**2** is responsible for its high g_{abs} (Figure 6c and 6d).

To further investigate the potential of these compounds as chiral emitters, the CPL spectra of enantiomers *P*/*M*-**1** and *P*/*M*-**2** were measured in chloroform (Figure 6b). In the CPL spectra, *P*- and *M*-enantiomers of **1** and **2** showed perfect mirror-image, consistent with their CD spectra. The g_{lum} of **2** reached to 2.3×10^{-3}, which is again about 4.5 times higher compared with that of **1** (5.0×10^{-4}). These results were further investigated by TD-DFT calculation performed at the ωB97XD/def2-svp level of theory. The calculated g_{lum} values of **1** and **2** are 4.3×10^{-4} and 1.8×10^{-3}, respectively, which are in good accordance with our experimental data (Table 2). Most reported neutral helicene emitters showed emission in the blue-greenish region. The CPL spectra up to 660 nm for **1** and 615 nm for **2** are among the most red-shifted well-resolved CPL spectra reported to date.[13, 54-56] The g_{lum}/g_{abs} value as a measure of the excited-state relaxation for **1** and **2** are significantly higher than that (0.61) obtained as a global average for all other reported helicenes and close to unity, demonstrating their structural rigidity endowed by naphthalimide annulation.[57] Following the suggestion of Zinna, the CPL brightness ($B_{CPL} = \epsilon_{max} \times \Phi_{PL} \times |g_{lum}|/2$) was used to evaluate the overall performance of CPL emitters.[13] The B_{CPL} of **1** and **2** were calculated to be 22.0 M^{-1} cm^{-1} and 66.5 M^{-1} cm^{-1}, respectively, which are among the highest values in the red-light region reported for all helicene derivatives in the literature, indicating that **2** could be an excellent emitter for CPL applications.

CONCLUSION

In conclusion, two naphthalimide-annulated [*n*]helicenes **1** and **2** were synthesized through a twofold palladium-catalyzed [3 + 3] annulation reaction in high yields. These compounds enrich the family of so far existing annulation products between naphthalimide units and various polycyclic aromatic cores as given in extended planar[58] or core-twisted[59] higher rylene bisimides, bowl-shaped corannulene bisimides[60] or zethrene bisimides[61] by annulation products bearing chiral aromatic helicene interconnectors. The structure of the new molecules was unambiguously proven by single-crystal X-ray diffraction analysis of enantiopure fractions of **1** and **2** obtained by chiral HPLC and the absolute configuration of the enantiopure fractions were assigned by X-ray structure analysis and comparison of measured and computed CD spectra. Both **1** and **2** exhibit outstanding fluorescence quantum yields of 73% and 69%, respectively, which are among the highest quantum yields reported for helicene derivatives in literature. We attribute these high quantum yields to the lateral annulation of naphthalimide moieties onto the [*n*]helicene that affords a high oscillator strength of the lowest energy transition. Moreover, the chiroptical properties of **1** and **2** were studied by CD and CPL spectroscopy. Approximately 4.5-fold enhancements in g_{abs} and g_{lum} were observed from **1** to **2** which could be attributed to the larger magnetic transition dipole moment of *P*-**2** by theoretical calculations. The CPL emission in the red spectral region up to 615 nm for **2** with superior B_{CPL} demonstrates that **2** is an excellent candidate for further investigations in chiral optoelectronics.[8]

ASSOCIATED CONTENT

Supporting Information. The Supporting Information is available free of charge on the ACS Publications website. Synthesis of all new compounds, UV/vis, fluorescence, NMR and mass spectra, details of X-ray diffraction experiments. (PDF).

Data Availability Statement. Additional data underlying this study are openly available in Zenodo at 10.5281/zenodo.7788788.

Accession Codes

CCDC 2195044, 2195046, 2195074, 2195075, and 2212687 contain the supplementary crystallographic data for this paper. These data can be obtained free of charge via www.ccdc.cam.ac.uk/data_request/cif, or by emailing

data_request@ccdc.cam.ac.uk, or by contacting The Cambridge Crystallographic Data Centre, 12 Union Road, Cambridge CB2 1EZ, UK; fax: +44 1223 336033.

AUTHOR INFORMATION

Corresponding Author

Frank Würthner − Institut für Organische Chemie, Universität Würzburg, 97074 Würzburg, Germany; Center for Nanosystems Chemistry (CNC), Universität Würzburg, 97074 Würzburg, Germany; orcid.org/0000-0001-7245-0471; Email: wuerthner@uni-wuerzburg.de

Authors

Xiaoqi Tian − Institut für Organische Chemie, Universität Würzburg, 97074 Würzburg, Germany

Kazutaka Shoyama − Institut für Organische Chemie, Universität Würzburg, 97074 Würzburg, Germany; orcid.org/0000-0003-0937-4431

Bernhard Mahlmeister − Center for Nanosystems Chemistry (CNC), Universität Würzburg, 97074 Würzburg, Germany

Felix Brust − Center for Nanosystems Chemistry (CNC), Universität Würzburg, 97074 Würzburg, Germany

Matthias Stolte − Institut für Organische Chemie, Universität Würzburg, 97074 Würzburg, Germany; Center for Nanosystems Chemistry (CNC), Universität Würzburg, 97074 Würzburg, Germany

Contributions

All authors have given approval to the final version of the manuscript.

Notes

The authors declare no competing financial interest.

ACKNOWLEDGMENT

This work was supported by Deutsche Forschungsgemeinschaft (DFG) (Grant WU 317/20-2). The authors are grateful to Prof. Agnieszka Nowak-Krol and Prof. Prince Ravat for sharing their chiral HPLC column and photoreactor, respectively. We thank the Alexander von Humboldt foundation for a postdoctoral stipend for Xiaoqi Tian. The CPL/CD hybrid spectrometer was funded by the Deutsche Forschungsgemeinschaft (DFG, German Research Foundation) – Projektnummer 444286426. We acknowledge DESY (Hamburg, Germany), a member of the Helmholtz Association HGF, for providing experimental facilities at PETRA III under P11 proposal No I-20211168 and STP-20010387. We thank Drs. Eva Crosas and Helena Taberman for assistance in using beamline P11.

REFERENCES

1. Shen, Y.; Chen, C. F., Helicenes: synthesis and applications. *Chem. Rev.* **2012,** *112* (3), 1463–1535.
2. Martin, R. H., The helicenes. *Angew. Chem. Int. Ed.* **1974,** *13*, 649–659.
3. Gingras, M., One hundred years of helicene chemistry. Part 1: non-stereoselective syntheses of carbohelicenes. *Chem. Soc. Rev.* **2013,** *42* (3), 968–1006.
4. Gingras, M.; Felix, G.; Peresutti, R., One hundred years of helicene chemistry. Part 2: stereoselective syntheses and chiral separations of carbohelicenes. *Chem. Soc. Rev.* **2013,** *42* (3), 1007–1050.
5. Takenaka, N.; Chen, J.; Captain, B.; Sarangthem, R. S.; Chandrakumar, A., Helical Chiral 2-Aminopyridinium Ions A New Class of Hydrogen Bond Donor Catalysts. *J. Am. Chem. Soc.* **2010,** *132*, 4536–4537.
6. Hassey, R.; Swain, E. J.; Hammer, N. I.; Venkataraman, D.; Barnes, M. D., Probing the Chiroptical Response of a Single Molecule. *Science* **2006,** *314*, 1437–1439.
7. Yang, Y.; da Costa, R. C.; Fuchter, M. J.; Campbell, A. J., Circularly polarized light detection by a chiral organic semiconductor transistor. *Nature. Photon.* **2013,** *7* (8), 634–638.
8. Zhang, L.; Song, I.; Ahn, J.; Han, M.; Linares, M.; Surin, M.; Zhang, H. J.; Oh, J. H.; Lin, J., π-Extended perylene diimide double-heterohelicenes as ambipolar organic semiconductors for broadband circularly polarized light detection. *Nat. Commun.* **2021,** *12* (1), 142.
9. Kelly, T. R., Progress toward a Rationally Designed Molecular Motor. *Acc. Chem. Res.* **2001,** *34*, 514–522.
10. Heffern, M. C.; Matosziuk, L. M.; Meade, T. J., Lanthanide probes for bioresponsive imaging. *Chem. Rev.* **2014,** *114* (8), 4496–4539.
11. Yang, Y.; da Costa, R. C.; Smilgies, D. M.; Campbell, A. J.; Fuchter, M. J., Induction of circularly polarized electroluminescence from an achiral light-emitting polymer via a chiral small-molecule dopant. *Adv. Mater.* **2013,** *25* (18), 2624−2628.
12. Brandt, J. R.; Wang, X.; Yang, Y.; Campbell, A. J.; Fuchter, M. J., Circularly Polarized Phosphorescent Electroluminescence with a High Dissymmetry Factor from PHOLEDs Based on a Platinahelicene. *J. Am. Chem. Soc.* **2016,** *138* (31), 9743–9746.
13. Arrico, L.; Di Bari, L.; Zinna, F., Quantifying the Overall Efficiency of Circularly Polarized Emitters. *Chem. Eur. J.* **2021,** *27* (9), 2920–2934.
14. Sapir, M.; Donckt, E. V., Intersystem crossing in the helicenes. *Chem. Phys. Lett.* **1975,** *36*, 108–110.
15. Birks, J. B.; Birch, D. J. S., Fluorescence of the higher helicenes. *Chem. Phys. Lett.* **1976,** *43*, 33–36.
16. Horrocks, A. R.; Wilkinson, F., Triplet state formation efficiencies of aromatic hydrocarbons in solution. *Proc. Roy. Soc. A.* **1968,** *306*, 257–273.
17. Englman, R.; Jortner, J., The energy gap law for radiationless transitions in large molecules. *Mol. Phys.* **1970,** *18*, 145–164.
18. Dhbaibi, K.; Favereau, L.; Crassous, J., Enantioenriched Helicenes and Helicenoids Containing Main-Group Elements (B, Si, N, P). *Chem. Rev.* **2019,** *119* (14), 8846–8953.
19. Oyama, H.; Nakano, K.; Harada, T.; Kuroda, R.; Naito, M.; Nobusawa, K.; Nozaki, K., Facile Synthetic Route to Highly Luminescent Sila[7]helicene. *Org. Lett.* **2013,** *15*, 2104–2107.
20. Kubo, H.; Hirose, T.; Matsuda, K., Control over the Emission Properties of [5]Helicenes Based on the Symmetry and Energy Levels of Their Molecular Orbitals. *Org. Lett.* **2017,** *19* (7), 1776–1779.
21. Schmidt, K.; Brovelli, S.; Coropceanu, V.; Beljonne, D.; Cornil, J.; Bazzini, C.; Caronna, T.; Tubino, R.; Meinardi, F.; Shuai, Z.; Brédas, J.-L., Intersystem Crossing Processes in Nonplanar Aromatic Heterocyclic Molecules. *J. Phys. Chem. A.* **2007,** *111*, 10490–10499.
22. Saal, F.; Zhang, F.; Holzapfel, M.; Stolte, M.; Michail, E.; Moos, M.; Schmiedel, A.; Krause, A. M.; Lambert, C.; Würthner, F.; Ravat, P., [*n*]Helicene Diimides (*n* = 5, 6, and 7):

Through-Bond versus Through-Space Conjugation. *J. Am. Chem. Soc.* **2020,** *142* (51), 21298–21303.
23. Cruz, C. M.; Castro-Fernandez, S.; Macoas, E.; Cuerva, J. M.; Campana, A. G., Undecabenzo[7]superhelicene: A Helical Nanographene Ribbon as a Circularly Polarized Luminescence Emitter. *Angew. Chem. Int. Ed.* **2018,** *57* (45), 14782–14786.
24. Reger, D.; Haines, P.; Heinemann, F. W.; Guldi, D. M.; Jux, N., Oxa[7]superhelicene: A π-Extended Helical Chromophore Based on Hexa-peri-hexabenzocoronenes. *Angew. Chem. Int. Ed.* **2018,** *57* (20), 5938–5942.
25. Fujikawa, T.; Segawa, Y.; Itami, K., Synthesis, Structures, and Properties of π-Extended Double Helicene: A Combination of Planar and Nonplanar π-Systems. *J. Am. Chem. Soc.* **2015,** *137* (24), 7763–7768.
26. Medel, M. A.; Tapia, R.; Blanco, V.; Miguel, D.; Morcillo, S. P.; Campana, A. G., Octagon-Embedded Carbohelicene as a Chiral Motif for Circularly Polarized Luminescence Emission of Saddle-Helix Nanographenes. *Angew. Chem. Int. Ed.* **2021,** *60* (11), 6094–6100.
27. Castro-Fernandez, S.; Cruz, C. M.; Mariz, I. F. A.; Marquez, I. R.; Jimenez, V. G.; Palomino-Ruiz, L.; Cuerva, J. M.; Macoas, E.; Campana, A. G., Two-Photon Absorption Enhancement by the Inclusion of a Tropone Ring in Distorted Nanographene Ribbons. *Angew. Chem. Int. Ed.* **2020,** *59* (18), 7139–7145.
28. Qiu, Z.; Ju, C. W.; Frederic, L.; Hu, Y.; Schollmeyer, D.; Pieters, G.; Müllen, K.; Narita, A., Amplification of Dissymmetry Factors in π-Extended [7]- and [9]Helicenes. *J. Am. Chem. Soc.* **2021,** *143* (12), 4661–4667.
29. Wu, Y. F.; Ying, S. W.; Su, L. Y.; Du, J. J.; Zhang, L.; Chen, B. W.; Tian, H. R.; Xu, H.; Zhang, M. L.; Yan, X.; Zhang, Q.; Xie, S. Y.; Zheng, L. S., Nitrogen-Embedded Quintuple [7]Helicene: A Helicene–Azacorannulene Hybrid with Strong Near-Infrared Fluorescence. *J. Am. Chem. Soc.* **2022,** *144* (24), 10736–10742.
30. Dubey, R. K.; Melle-Franco, M.; Mateo-Alonso, A., Inducing Single-Handed Helicity in a Twisted Molecular Nanoribbon. *J. Am. Chem. Soc.* **2022,** *144* (6), 2765–2774.
31. Weiss, C.; Sharapa, D. I.; Hirsch, A., Coronenohelicenes with Dynamic Chirality. *Chem. Eur. J.* **2020,** *26* (62), 14100–14108.
32. Dhbaibi, K.; Favereau, L.; Srebro-Hooper, M.; Quinton, C.; Vanthuyne, N.; Arrico, L.; Roisnel, T.; Jamoussi, B.; Poriel, C.; Cabanetos, C.; Autschbach, J.; Crassous, J., Modulation of circularly polarized luminescence through excited-state symmetry breaking and interbranched exciton coupling in helical push-pull organic systems. *Chem. Sci.* **2020,** *11* (2), 567–576.
33. Schuster, N. J.; Paley, D. W.; Jockusch, S.; Ng, F.; Steigerwald, M. L.; Nuckolls, C., Electron Delocalization in Perylene Diimide Helicenes. *Angew. Chem. Int. Ed.* **2016,** *55* (43), 13519–13523.
34. Schuster, N. J.; Hernandez Sanchez, R.; Bukharina, D.; Kotov, N. A.; Berova, N.; Ng, F.; Steigerwald, M. L.; Nuckolls, C., A Helicene Nanoribbon with Greatly Amplified Chirality. *J. Am. Chem. Soc.* **2018,** *140* (20), 6235–6239.
35. Milton, M.; Schuster, N. J.; Paley, D. W.; Hernandez Sanchez, R.; Ng, F.; Steigerwald, M. L.; Nuckolls, C., Defying strain in the synthesis of an electroactive bilayer helicene. *Chem. Sci.* **2019,** *10* (4), 1029–1034.
36. Schuster, N. J.; Joyce, L. A.; Paley, D. W.; Ng, F.; Steigerwald, M. L.; Nuckolls, C., The Structural Origins of Intense Circular Dichroism in a Waggling Helicene Nanoribbon. *J. Am. Chem. Soc.* **2020,** *142* (15), 7066–7074.
37. Xiao, X.; Pedersen, S. K.; Aranda, D.; Yang, J.; Wiscons, R. A.; Pittelkow, M.; Steigerwald, M. L.; Santoro, F.; Schuster, N. J.; Nuckolls, C., Chirality Amplified: Long, Discrete Helicene Nanoribbons. *J. Am. Chem. Soc.* **2021,** *143* (2), 983–991.
38. Liu, B.; Bockmann, M.; Jiang, W.; Doltsinis, N. L.; Wang, Z., Perylene Diimide-Embedded Double [8]Helicenes. *J. Am. Chem. Soc.* **2020,** *142* (15), 7092–7099.
39. Jiang, W.; Wang, Z., Molecular Carbon Imides. *J. Am. Chem. Soc.* **2022,** *144* (33), 14976–14991.
40. Pigulski, B.; Shoyama, K.; Sun, M. J.; Würthner, F., Fluorescence Enhancement by Supramolecular Sequestration of a C54-Nanographene Trisimide by Hexabenzocoronene. *J. Am. Chem. Soc.* **2022,** *144* (13), 5718–5722.
41. Seifert, S.; Shoyama, K.; Schmidt, D.; Würthner, F., An Electron-Poor C64 Nanographene by Palladium-Catalyzed Cascade C–C Bond Formation: One-Pot Synthesis and Single-Crystal Structure Analysis. *Angew. Chem. Int. Ed.* **2016,** *55* (22), 6390–6395.
42. Yuan, L.; Lin, W.; Zheng, K.; He, L.; Huang, W., Far-red to near infrared analyte-responsive fluorescent probes based on organic fluorophore platforms for fluorescence imaging. *Chem. Soc. Rev.* **2013,** *42* (2), 622–661.
43. Liu, M.; Zhang, L.; Wang, T., Supramolecular Chirality in Self-Assembled Systems. *Chem. Rev.* **2015,** *115* (15), 7304–7397.
44. Ravat, P.; Hinkelmann, R.; Steinebrunner, D.; Prescimone, A.; Bodoky, I.; Juricek, M., Configurational Stability of [5]Helicenes. *Org. Lett.* **2017,** *19* (14), 3707–3710.
45. Yang, B.; Liu, L.; Katz, T. J.; Liberko, C. A.; Miller, L. L., Electron delocalization in helical quinone anion radicals. *J. Am. Chem. Soc.* **1991,** *113*, 8993–8994.
46. Liu, L.; Yang, B.; Katz, T. J.; Poindexter, M. K., Improved Methodology for Photocyclization Reactions. *J. Org. Chem.* **1991,** *56*, 3769–3775.
47. Mori, K.; Murase, T.; Fujita, M., One-step synthesis of [16]helicene. *Angew. Chem. Int. Ed.* **2015,** *54* (23), 6847–6851.
48. Organ, M. G.; Abdel-Hadi, M.; Avola, S.; Hadei, N.; Nasielski, J.; O'Brien C, J.; Valente, C., Biaryls made easy: PEPPSI and the Kumada–Tamao–Corriu reaction. *Chem. Eur. J.* **2007,** *13* (1), 150–157.
49. Ghosh, A. K.; Cheng, X.; Zhou, B., Enantioselective Total Synthesis of (+)-Lithospermic Acid. *Org. Lett.* **2012,** *14*, 5046–5049.
50. Ivanova, B. B.; Spiteller, M., Noncentrosymmetric Crystals with Marked Nonlinear Optical Properties. *J. Phys. Chem. A.* **2010,** *114*, 5009–5103.
51. Lee, S. K.; Zu, Y.; Herrmann, A.; Geerts, Y.; Müllen, K.; Bard, A. J., Electrochemistry, Spectroscopy and Electrogenerated Chemiluminescence of Perylene, Terrylene, and Quaterrylene Diimides in Aprotic Solution. *J. Am. Chem. Soc.* **1999,** *121*, 3513–3520.
52. Kubo, H.; Hirose, T.; Nakashima, T.; Kawai, T.; Hasegawa, J. Y.; Matsuda, K., Tuning Transition Electric and Magnetic Dipole Moments: [7]Helicenes Showing Intense Circularly Polarized Luminescence. *J. Phys. Chem. Lett.* **2021,** *12* (1), 686–695.
53. Schellman, J. A., Circular dichroism and optical rotation. *Chem. Rev.* **1975,** *75*, 323–331.

54. Dhbaibi, K.; Favereau, L.; Srebro-Hooper, M.; Jean, M.; Vanthuyne, N.; Zinna, F.; Jamoussi, B.; Di Bari, L.; Autschbach, J.; Crassous, J., Exciton coupling in diketopyrrolopyrrole-helicene derivatives leads to red and near-infrared circularly polarized luminescence. *Chem. Sci.* **2018,** *9* (3), 735–742.
55. Dhbaibi, K.; Matozzo, P.; Abella, L.; Jean, M.; Vanthuyne, N.; Autschbach, J.; Favereau, L.; Crassous, J., Exciton coupling chirality in helicene-porphyrin conjugates. *Chem. Commun.* **2021,** *57* (82), 10743–10746.
56. Bosson, J.; Labrador, G. M.; Jacquemin, D.; Lacour, J., Cationic [6]Helicenes: Tuning (Chir)Optical Properties up to the Near Infra-Red. *Mater. Today:. Proc.* **2022,** *62*, 7751–7753.
57. Tanaka, H.; Inoue, Y.; Mori, T., Circularly Polarized Luminescence and Circular Dichroisms in Small Organic Molecules: Correlation between Excitation and Emission Dissymmetry Factors. *ChemPhotoChem.* **2018,** *2* (5), 386–402.
58. Chen, L.; Li, C.; Müllen, K., Beyond perylene diimides: synthesis, assembly and function of higher rylene chromophores. *J. Mater. Chem. C* **2014,** *2* (11), 1938–1956.
59. Mahlmeister, B.; Mahl, M.; Reichelt, H.; Shoyama, K.; Stolte, M.; Würthner, F., Helically Twisted Nanoribbons Based on Emissive Near-Infrared Responsive Quaterrylene Bisimides. *J. Am. Chem. Soc.* **2022,** *144* (23), 10507–10514.
60. Renner, R.; Menekse, K.; Mahlmeister, B.; Stolte, M.; Würthner, F., Bowl-Shaped Naphthalimide-Annulated Corannulene as Nonfullerene Acceptor in Organic Solar Cells. *Organic Materials* **2020,** *02* (03), 229–234.
61. Sun, Z.; Huang, K. W.; Wu, J., Soluble and stable heptazethrenebis(dicarboximide) with a singlet open-shell ground state. *J. Am. Chem. Soc.* **2011,** *133* (31), 11896–11899.